

PROBING TIME- AND SPATIAL-RESOLVED MAGNETIZATION DYNAMICS DRIVEN BY SPIN-ORBIT TORQUES

#1SRI PERUMBUDUR RAMKUMAR, *Assistant Professor*

#2ANUSHA BANDI, *Assistant Professor*

#3THOTA JAMUNA, *Assistant Professor*

Department of Humanities and Science(Physics),

SREE CHAITANYA INSTITUTE OF TECHNOLOGICAL SCIENCES, KARIMNAGAR, TS.

ABSTRACT: Spin-orbit torques (SOTs) caused by current are a powerful tool for spintronic device magnetization reduction. Nonvolatile memory and logic devices find SOTs particularly appealing for fast switching applications due to their orthogonal torque-magnetization configuration, considerable damping, and higher domain wall velocities, which are traits of materials with superior spin-orbit coupling. However, the exact moment and progression of magnetism during switching is still unclear. Initial findings of spin-orbit torque-driven magnetization dynamics in Pt/Co/AlO_x nanoparticles injected with current pulses are presented here. The switching seen during a sub-nanosecond current pulse is explained by the rapid formation of an inverted domain at the dot's edge and the propagation of a slanted domain wall across the dot, as shown by time-resolved x-ray images with a spatial resolution of 25 nm and a temporal resolution of 100 ps. Depending on the polarity of the external field, current, and magnetism, the nucleation position varies across the four dot quadrants. The synergistic effect of field-like and damping-like spin-orbit torques breaks magnetic symmetry, as shown by our data, allowing credible switching events lasting more than 10^{12} reversal cycles.

1. INTRODUCTION

To create nonvolatile memory devices that use little static and dynamic power, it is essential to regulate the magnetic state of thin heterostructures using electric currents. An interesting technique for magnetic switching involves injecting an in-plane current into a bilayer of ferromagnets and heavy metals. An efficient way to manage domain barriers and reverse magnetization is via the spin-orbit torques (SOTs) produced by the interface charge-spin conversion and the spin Hall effect. Whether the SOT switching systems are magnetized in-plane or out-of-plane, three-terminal magnetic tunnel junctions can readily handle them.

Despite being much larger in scale than the two-terminal spin-transfer torque (STT) technology currently used in magnetic random

access memory (MRAM), the three-terminal architecture gives the desired properties. The separation of the read and write current channels of the tunnel junction is this characteristic that allows independent tunneling magneto resistance optimization during reading and eliminates electrical stress on the oxide barrier during writing.

The SOTs are produced by spin accumulation that is perpendicular to the quiescent magnetization, leading to a very small incubation delay. Because of this, lightning-fast performance is also essential. The switching time distribution caused by thermal fluctuations is several nanoseconds in scope, making this kind of delay a major concern for STT devices. In addition, strong attenuation in the monodomain regime and fast domain wall motion in the multidomain regime both affect

the dynamics of SOT-induced magnetization, which allows for the fast reversal of magnetism.

Recent studies on SOTs in ferromagnetic/heavy metal layers have shown that Pt/Co and Ta/CoFeB structures can be reliably switched using current pulses as brief as 200 ps. Studies like these only looked at the switching probability as a function of pulse length and intensity; the exact mechanism and timing of magnetization reversal are still mysteries. A thorough examination of SOT-induced DW displacements employing magneto-optic Kerr effect microscopy revealed the role of the Dzyaloshinskii-Moriya interaction (DMI) in stabilizing chiral DW structures with very high mobility. Following current injection, these investigations, which were comparable to intermittent switching trials, focused on stationary magnetization at a spatial resolution of about 1 μm . Concurrent with this work, a plethora of theoretical models have been put out in an effort to shed light on the dynamics caused by SOT. The most basic answer is given by the macrospin approximation, which is valid for tiny magnets with coherent magnetization rotation.

The field-like torque $\text{TFL} \parallel \dot{M}_y$, which is orthogonal to the current, causes the magnetization to precess around the y-axis under certain assumptions. On the other hand, the magnetization is rotated by the damping-like (DL) torque $\text{TDL} \propto M \times (y \times M)$. Although the reverse mode is still up for debate, this model is commonly used in real devices to link the SOT amplitude to the required switching current. In the second model, a thermally accelerated DW depinning mechanism and the DL component of the SOT³⁶ are used to produce magnetic bubbles that expand isotropically and randomly.

At the sample edge, where domain nucleation is both random and thermally aided, micromagnetic models have also been created. In these models, the conflict between the external field and DMI causes DW to propagate throughout the magnetic layer. As a z-axis field ($\text{BDL} \propto M_x$) in perpendicularly magnetic

layers, the internal DW magnetization is impacted by the DL torque. The up-down DW of the type $\downarrow \leftarrow \downarrow$ promotes domain extension on the side with a greater $|M_x|$, in contrast to the down-up DW of the opposite direction, $\downarrow \rightarrow \uparrow$. Many obstacles remain despite these admirable efforts. Among these are the magnetic configurations that exist before and during the switching process, the role that the DL and FL torque and DMI components play, and the physical and temporal processes that influence the dynamics of magnetization before and after current injection. For current-pump and x-ray probe investigations in the temporal domain, we report direct observation of the dynamics produced by SOTs during switching using a scanning transmission x-ray microscope (STXM).

Depending on the amplitude and duration of the current pulses, our research shows that the nanoscale magnetization changes from the early domain nucleation stage to full or partial switching. That which is specific to SOTs—the interaction between the external magnetic field, DMI, and current-induced torques—defines the contrary direction. The real switching speed is confirmed by these results.

Four different configurations of nucleation sites and fast DW propagation paths are found in agreement with the four possible combinations of current and field polarization. By combining STXM data with micromagnetic simulations and all-electrical switching probability measurements, a consistent picture of the switching process is created, revealing how the reversal route is affected by the FL torque, DL torque, and DMI. In conclusion, we have demonstrated that switching offers great promise for SOTs in MRAM devices due to its resistance to sample magnetic structure flaws and repetitive cycle occurrences.

2. TIME-RESOLVED SWITCHING

In this study, we analyzed 500 nm in diameter and 1 nm thick circular Co specks magnetized perpendicularly. They are topped with 2 nm AlO_x and laid on a Pt current line that is 750 nm broad and 5 nm thick. Figure 1c shows the

samples that were made using electron-beam lithography on x-ray transmitting transparent Si₃N₄ membranes that were linked by Au leads. Si₃N₄ membranes were used to print out copies of the dots with four electrical contacts for all-electric pulsed switching.

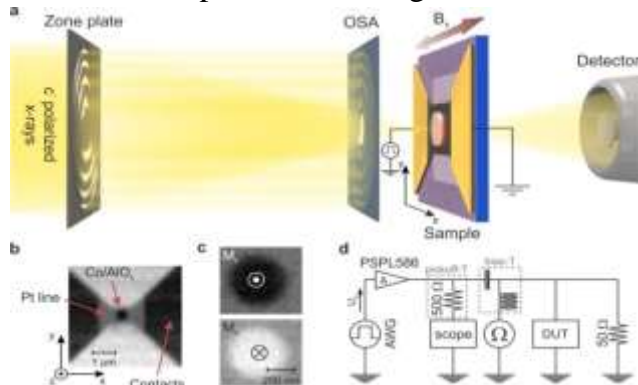
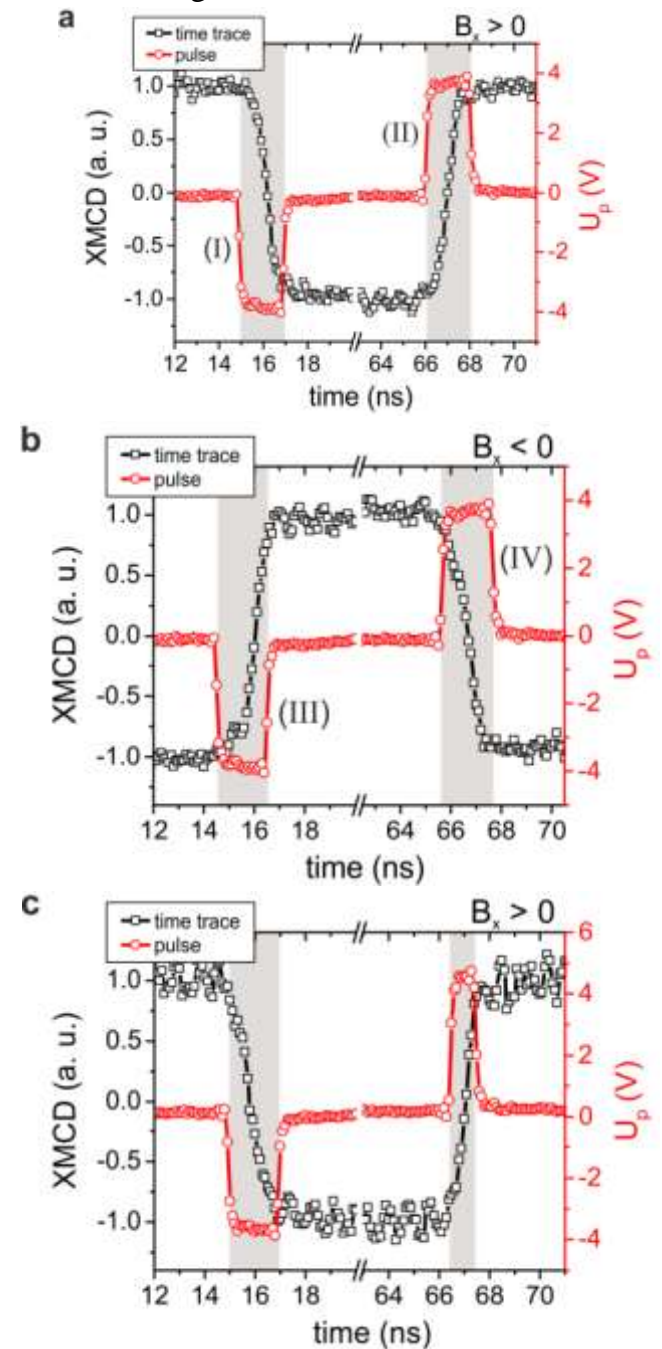


Figure 1: The graphic shows the structure of the sample and the experimental instrument. By utilizing an order selecting aperture (OSA) and a zone plate, a 25 nm point is focused on by means of a circularly polarized x-ray beam. An avalanche photodiode records the x-rays' passage as the sample stage is scanned across the x-ray focus in 12-to 25-nanometer intervals. b) An example of a representative STXM image showing elemental and topographic contrast, with a Co dot and a Pt line at 779 eV. In the darker areas, you can see the Au contact pads and Co dot, which absorb x-rays more strongly than the bare Pt and Si₃N₄ parts. c) Magnetization in relation to the x-ray helicity determines the absorption amplitude in the XMCD effect-induced magnetic contrast. To show that $M_z > 0$ (or that $M_z < 0$), a black-and-white contrast is employed. d, Pump current circuit diagram.

In addition to SOT measurement, Hall bar constructions are also provided (see supplemental info). Figure 1b shows the result of scanning the sample under the focused x-ray beam, which produced a static image of the Pt line and Co dot. The transmitted x-ray intensity at the Co L₃ absorption edge was studied stroboscopically to provide time-resolved pictures of the Co magnetization, as shown in Fig. 1c. A comparison is made between x-ray magnetic circular dichroism (XMCD) and the out-of-plane component of magnetization (M_z). With a period of 102.1 ns, or about 20 MHz

switching rate, the pump current consists of a series of negative (set) and positive (reset) pulses of variable duration and amplitude. Unconventionally, the switching polarity was specified by applying an in-plane magnetic field B_x along the current channel 9.



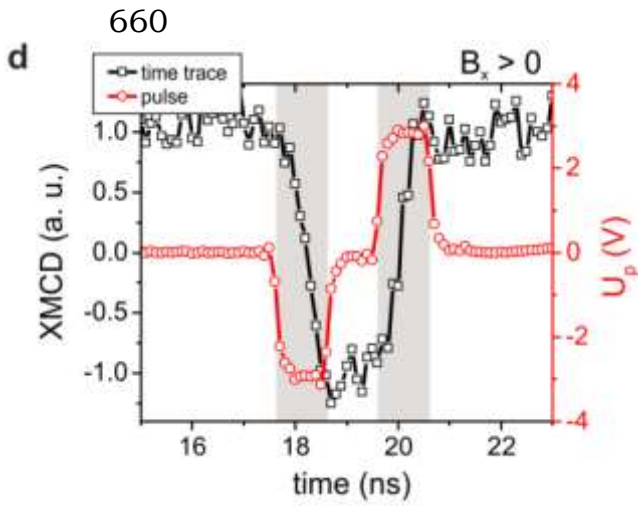


Figure 2: There is a relationship between the resolution of time and the fluctuations in magnetization. The XMCD time traces at a, $B_x = 94$ mT and b, $B_x = -124$ mT show that an injection of 2 ns long opposite-polarity current pulses causes the magnetization to invert. When M_z is negative, the XMCD signal is positive; when M_z is positive, it is negative. c, A slightly off set set-reset sequence with an initial event pulse of two nanoseconds and a subsequent event pulse of 0.8 nanoseconds. d, a fast-switching sequence with an in-plane field $B_x = 92$ mT, featuring two 1-ns long current pulses of polarity opposite to one another, spaced 1 ns apart. On the Pt line, the current density $j_p = 8.4 \times 10^7$ A/cm² is the same as $U_p = 1$ V.

In addition to the sample, a fast oscilloscope acquired the XMCD time trace independently, as shown in Figure 2a. This trace was generated by integrating the transmitted x-ray intensity over the whole Co dot region during the current pulse sequence. The individual pulses in this sequence have a 2 ns duration, a rising time of about 150 ps, and a spacing of 50 ns. Magnetization moves downwards during the first (negative) pulse and upwards during the second (positive), according to the XMCD time trace.

The duration of the current pulses and the time it takes for M_z to transition between two states with opposing saturation magnetization demonstrate that there is no delayed or after-pulse relaxation and that the magnetization is completely reversed during the pulse interval. Figure 2b shows that when the sign of B_x changes, the magnetization's response to

current pulses inverts. Previous work on the inversion of perpendicularly magnetic layers caused by SOT confirms this. Furthermore, we found that a complete magnetization during a sub-ns current pulse is possible by raising the current amplitude, which in turn increases the switching speed (Fig. 2c).

The lack of negative effects and the extremely high speed make magnetic writing cycles possible. Figure 2d shows an example of such a cycle, which switches the magnetization from a down to an up state using a pulse sequence of 1 ns on, 1 ns off, and 1 ns on. Our samples show no noticeable electrical or magnetic degradation after hours of continuous pulse sequences, which is quite remarkable. Over ten thousand switching occurrences were successfully tested at current densities ranging from 2 to 4 x 10⁷ A/cm². Our results show that SOT-based MRAM and logic devices perform admirably due to their combination of speed and durability.

As a result of injecting current, magnetization moves forward in space. Next, we have a look at the processes that cause a reversal of magnetization as well as temporary magnetic configurations. Figure 3a shows four sets of sequential images taken at 100 ps intervals during the switching process. These photographs show the four possible combinations of field polarity and current. There is no noticeable incubation delay and magnetization always reverses due to domain nucleation and propagation. The reversal process appears to be predictable and repeatable, as shown by a distinct DW front that moves across the sample from a fixed nucleation point on one side to the other (red dots and green arrows in Fig. 3a), even though our observations are stroboscopic. Because of this, we are unable to study random effects.

Plus, we'll argue in the next part that SOTs are the only things with that kind of reversal scheme. We confirm the predictions of earlier micromagnetic models by showing that domain nucleation occurs at the sample's

edge, where the DMI and Bx collaborate to change the magnetization along the current direction. The domain nucleation site, which already exhibits an extra top/bottom asymmetry, rotates between the four quadrants shown in Figure 3b. But when BDL, DMI, and Bx work together, the only thing that happens is a left/right asymmetry, which is the same as when a perpendicular magnetic field produces asymmetric nucleation.

3. EDGE NUCLEATION

In order to comprehend this additional imbalance, it is imperative that we conduct a more thorough examination of the impacts of static and dynamic fields. The left-handed N'eel-DW is stabilized by the canting of the magnetization at the dot's edge, which is caused by the positive DMI of Pt/Co/AlOx. In the absence of both external field and current, the magnetic moments for $M_z > 0$ ($M_z < 0$) are symmetrically canted inward (outward) of the dot, as demonstrated.

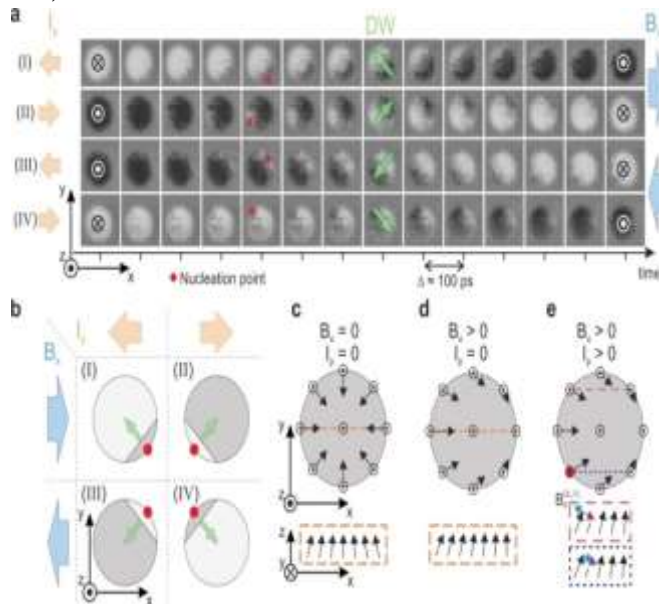


Figure 3: Changes occur to magnetization as the switching process progresses. While administering a 2 ns current pulse, images were captured at 100 ps intervals. Rows I, II, and III of Figures 2a and 2b show the time traces, correspondingly. The green arrows show the direction of propagation, whereas the red spots indicate the position of the DW nucleation. Improving contrast is the job of a low-pass filter. b, Artistic representation of the measured geometry of nucleation and propagation

of domain walls. Here we see an example of the DW nucleation method in action in Case II: Configurations C and D produce magnetization through dot edge canting due to magneto-ionic processes. A and Bx break the canting symmetry. Figure 3c shows how BDL and BFL work. When a stationary field Bx is supplied, the canting angle increases on one side and decreases on the other, causing domain nucleation to occur on the side with the greater canting angle (Fig. 3d). The polar component BDL is aligned with the direction of the current when a positive current pulse is applied, resulting in an effective DL field (purple arrow in Fig. 3e). That is why, when $M_z > 0$, BDL causes left nucleation for positive Bx, and when $M_z < 0$, no nucleation happens for positive Bx. Every one of the four possible configurations of field and current polarity that cause magnetization switching can have its corresponding left/right data imbalance explained by logical explanation. However, the top/bottom asymmetry can only be proven if an extra torque has a large impact on the nucleation process. Next, we state that the FL torque and DMI-induced canting at the sample edges are the sources of the asymmetry. The relevant effective field consists of BFL points.

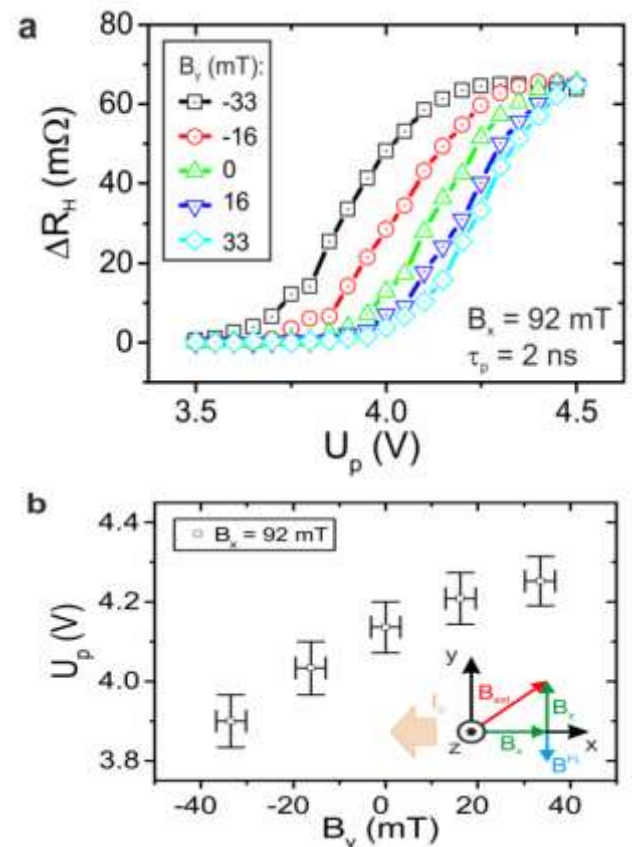


Figure 4: A counter-force from the outside world acts on the FL torque. By comparing

the Hall resistance before and after the pulse with respect to the applied voltage, the change in magnetization can be evaluated. A direct correlation exists between the percentage of dot area displaying reversed magnetization and the external fields B_y , in both the up-plane and in-plane directions. Over 200 switching events, the average of ΔRH was calculated. The relationship between the threshold voltage and B_y at 50% switching. At 92 mT, the x-component of the electrostatic field is defined. In the inset, you can see the graphic that shows the field direction. At times, models that account for SOT-induced dynamics in domain walls fail to take this torque into account. This is because, for B_y values greater than zero ($B_y < \text{zero}$), it compensates for BFL in the y-direction, and it does not project down the easy axis.

The direction of the polar component BFL $\propto M_z M_y / \sin \theta$, which points upward or downward depending on the sign of M_y , is indicated by the blue arrows in Fig. 3e. The formation of a reverse domain and the rotation of magnetization are enhanced when BFL and BDL are parallel, as shown by the red dots in Figure 3. When they are in opposition to one another, they create obstacles. Our samples' harmonic Hall voltage measurements of the FL and DL torques, as well as macrospin and micromagnetic models that include these torques (see Supplementary Information), lend credence to this qualitative claim. The amplitudes of BFL and BDL, as shown in the simulations, are around 20 mT per 108 A/cm². This instance is consistent with the theory that the z-component of the Oersted field, which is generated by the current through the Pt line, can enhance nucleation and produce a top/bottom asymmetry similar to the one seen. We have determined that Oersted field-assisted switching has minimal impact in this scenario, despite its allure for device applications. This occurs because the Oersted field is much smaller than the FL torque, and the closest edge of the Co dot is

just 125 nm from the current line (see to the supplementary material for details).

4. FL TORQUE PROMOTES SWITCHING EFFICIENCY

We conducted all-electrical pulsed switching experiments on the replica Pt/Co/AlO_x dots in the presence of an extra in-plane field B_y , applied parallel or antiparallel to BFL, to gain a more comprehensive understanding of the impact of the FL torque on the reversal process.

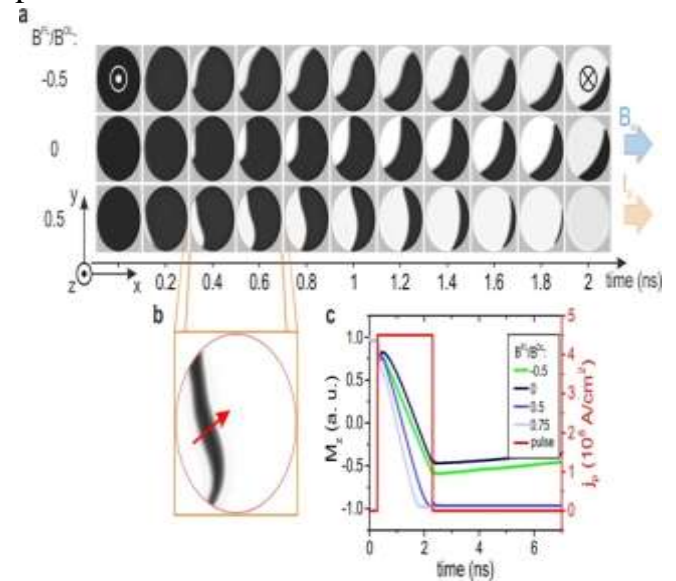


Figure 5: Micromagnetic simulations of the reversal process. Images of the magnetic arrangement were obtained at various points in time. A diverse array of FL torque-to-DL torque ratios is implemented in the simulations. b, The inclination of the DW is indicated by the contrast difference between two subsequent frames. The inverted domain's extent is illustrated by the shadowy region. c, Time trace simulation of the perpendicular magnetization component during transition.

The anomalous Hall effect is implemented to ascertain the dot's netization subsequent to each current pulse injection. The change in Hall resistance measured after injecting negative pulses with increasing amplitude over a range of B_y values is depicted in Figure 4a. As demonstrated by the shift of the various curves, a negative B_y , which is parallel to BFL and antiparallel to the in-plane component of the Oersted field, promotes switching, whereas a positive B_y inhibits it. This is most clearly

demonstrated by the voltage threshold at which 50% of the dot's magnetization reverses (Fig. 4b). The conclusions derived from the nucleation point investigation are corroborated by these findings, which demonstrate that the FL torque is essential for initiating the reverse process and enhancing switching efficiency.

Dynamic propagation of domain barriers The inclination of the propagating DW front in relation to the direction of the current is a notable feature of Figure 3. Depending on the current sign and DW configuration (up/down or down/up), the inclination angle varies from 45° to 90° . Current-induced DW tilting is a reliable indicator of the DMI in perpendicular magnetized nanotracks, as demonstrated by a recent study^{30,33}. The inclination angle in Fig. 3 is not consistent with the predictions of MOKE microscopy and micromagnetic models of Pt/Co heterostructures.

At a positive current, the angle between the DW normal and the current direction is approximately -45° for a left-handed up-down DW ($\uparrow\leftarrow\downarrow$), as opposed to $\approx +45^\circ$ as previously stated (refer to panel IV in Fig. 3b). We are of the opinion that the time-resolved nature of our data and the disregard for FL torque in micromagnetic models of current-induced DW motion are the causes of this disparity. The internal DW magnetization is rotated away from the x-axis to restore the DMI's preferred Néel configuration, as the tilt angle of the Pt/Co/AlOx spots is comparable to that of an external in-plane magnetic field B_y .

Our micromechanical simulations, which incorporate BFL in addition to BDL and DMI, accurately replicate the dynamic inclination observed during DW propagation, as illustrated in Fig. 5. Additionally, simulations demonstrate that the propagation of DW is enhanced by FL torque in the direction denoted by the arrow in Fig. 5b. This is consistent with scenario II, as illustrated in Fig. 3, and may also account for the significant anisotropy in DW velocity observed in extended Pt/Co/AlOx layers¹⁵. We also observe that the DW velocity increases as B_x increases; however, the bias field B_x does not alter the DW propagation direction. This

field is primarily used to disrupt the spin-canting symmetry generated by the DMI (see Supplementary Information).

The opposite DW tilt observed in this system compared to the Pt/Co/Ni/Co racetracks may be attributed to the shifting SOT amplitudes, as the tilt angle is determined by the BFL/BDL ratio. The more significant distinction is that we examine the dynamic structure of the DW during current injection, rather than after the current-induced displacement. Beginning with a homogeneous magnetization state, we envision the fastest DW front racing across the sample with the opposite tilt to the slowest DW front that persists in steady state conditions.

Consequently, we have determined that the direction of the highest DW velocity recently reported for Pt/Co/AlOx¹⁵ is orthogonal to the DW front in our data. These results demonstrate that the domain nucleation symmetry and DW propagation direction collaborate to enhance magnetization switching in the Pt/Co/AlOx dots, enabling the fastest DW front to sweep effortlessly across the entire dot extension. In order to illustrate a less favorable scenario (Fig. 5a), we implemented a negative BFL simulation. The domain nucleation point is relocated to the opposite periphery of the dot by the field, resulting in reversal dynamics that are significantly slower, despite the fact that the direction of DW propagation down the x-axis remains constant. Partial transition, sub-threshold current amplitude. We estimate the DW velocity to be approximately 400 m/s and derive the time required for the DW front to cover the central region of the dots using quasi-static observations of DW displacements. This is equivalent to approximately 100 m/s for each 108 A/cm² of injected current. Only one individual is capable of completing magnetization reversal due to its predictable nature.

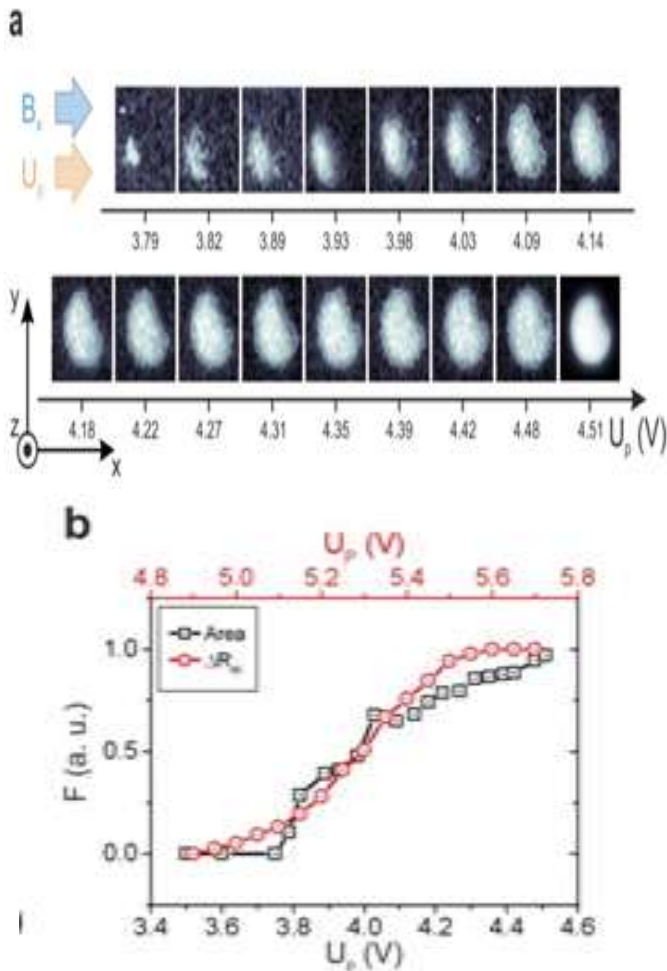


Figure 6: Incomplete switching is the consequence of pulses of subthreshold current. A, Differential images of voltage amplitude pulses that increase, illustrating the extent of magnetization reversal (in white). To determine the differential contrast, subtract the average of all frames after negative pulse injection from the average of all frames in a time-sequence after positive pulse injection. B, A comparison of the fractional reversed area computed from the photos in a with the all-electrical switching determined by Hall resistance on a replica dot. The Hall resistance data is averaged using 200 pulse cycles. The current dispersion in the Hall cross branches, which is absent in STXM measurements, is the cause of the discrepancy in voltage scales between the two investigations.

The switching timescale for the aggregate sample should be proportional to the size of the lateral samples. Switching periods can be as low as 200 ps in structures that are smaller than 100 nm. Additionally, we observe that pulses with amplitudes that are either lower or shorter than the threshold values necessary for full

switching routinely reverse a portion of the dot area. The results of a succession of switching experiments conducted on the current line at progressively higher voltage levels are illustrated in Figure 6a.

Each frame is a differential image that displays the average dot area when positive and negative pulses are applied, resulting in a reversible shift in magnetization. The critical switching current is more significantly influenced by the DW mobility and sample size than by the initial nucleation barrier, as illustrated in Fig. 6b. The reversed dot area is closely correlated with the remanent magnetization, as determined by the anomalous Hall effect on a replica dot, which increases monotonically with the pulse amplitude.

Additionally, our results corroborate the rapid attenuation of magnetic excitations in SOT devices, the absence of DW inertia observed in Pt/Co layers, and the possibility of achieving partial but dependable switching even when operating at a current amplitude that is less than the minimum required for full switching.

4. CONCLUSION

Controlling the rate at which electrical currents transition magnetically is one of the most challenging aspects of nonvolatile memory technology. We observed persistent sub-ns magnetization reversal of perpendicularly magnetized Pt/Co spots generated by SOTs over more than 1012 switching cycles. A four-fold asymmetry in the domain nucleation site at the dot edge and in the DW propagation direction is revealed by time-resolved STXM, which is contingent upon the relative alignment of the current and external field. This insight provides a previously unknown perspective on the spatial evolution of the magnetization and SOT-induced dynamics during the reversal process. The rapid direction of DW motion is diagonal to the current, in contrast to the steady-state direction observed in racetrack structures. Our results are supported by pulsed switching Hall measurements and micromagnetic computations, in addition to the DL torque and DMI, suggesting that the FL

torque exerts an impact on DW dynamics and nucleation. The efficiency of SOT switching can be enhanced by either designing structures with a large Oersted field or by adjusting the amplitude and sign of the FL torque independently of the DL torque. Additionally, the timing and quantity of magnetization reversal can be precisely controlled by adjusting the amplitude and duration of the current pulses, as well as the sample size, due to the predictable and deterministic nature of the switching process.

REFERENCES

1. Manchon, A., et al. (2020). Spin-Orbit Torques: Advances and Perspectives. *Nature Materials*, 19(10), 1012–1023.
2. Liu, L., et al. (2021). Spatiotemporal Observation of Magnetization Dynamics in Multilayers with Strong Spin-Orbit Coupling. *Physical Review Letters*, 126(14), 146802.
3. Ramaswamy, R., et al. (2020). Recent Advances in Spin-Orbit Torques in Magnetic Heterostructures. *Applied Physics Reviews*, 7(1), 011305.
4. Kim, J., et al. (2022). Time-Resolved Magnetization Dynamics Driven by Current-Induced Spin-Orbit Torques. *Nature Communications*, 13, 428.
5. Baek, S. C., et al. (2023). Visualizing Spin-Orbit Torque-Induced Magnetization Switching with Ultrafast Microscopy. *Science Advances*, 9(2), eabq0020.
6. Avci, C. O., et al. (2021). Spatio-Temporal Control of Magnetic Skyrmions via Spin-Orbit Torques. *Nano Letters*, 21(9), 3910–3917.
7. Heinonen, O., et al. (2020). Modeling Time-Resolved Magnetization Dynamics under Spin-Orbit Torque Influence. *Journal of Applied Physics*, 128(19), 191101.
8. Hayashi, M., et al. (2022). Current-Induced Dynamics of Domain Walls and Spin-Orbit Torques in Ferromagnetic Nanowires. *Nature Nanotechnology*, 17, 566–574.
9. Barker, J., et al. (2020). Impact of Spin-Orbit Torque on Magnetization Precession. *IEEE Transactions on Magnetics*, 56(11), 6100207.
10. Fukami, S., et al. (2023). Spin-Orbit Torques

JNAO Vol. 14, Issue. 2, : 2023
in Heavy Metal/Ferromagnet Heterostructures: Experimental Insights. *Advanced Functional Materials*, 33(3), 2204998.

11. Zhang, X., et al. (2022). Ultrafast Spin Dynamics Induced by Spin-Orbit Torques in Ferrimagnetic Alloys. *Physical Review B*, 106(17), 174410.
12. Kurebayashi, H., et al. (2020). Spin-Orbit Interaction-Driven Magnetization Dynamics in Antiferromagnets. *Journal of Magnetism and Magnetic Materials*, 504, 166636.
13. Taniguchi, T., et al. (2021). Analysis of Time-Resolved Magnetization Reversal in Spin-Orbit Torque Devices. *Journal of Physics D: Applied Physics*, 54(35), 355004.
14. Bhatti, S., et al. (2022). Spatially Resolved Imaging of Spin-Orbit Torque Switching in Nanostructures. *Nature Physics*, 18, 983–988.
15. Shiota, Y., et al. (2024). Time-Resolved X-Ray Spectroscopy of Spin-Orbit Torque Phenomena in Ferromagnets. *Advanced Materials*, 36(2), 2306712.